Appl Phys A
DOI 10.1007/s00339-009-5307-y

Applied Physics A
Materials Science & Processing

LiFAP-based PVdF–HFP microporous membranes by phase-inversion technique with Li/$LiFePO_4$ cell

V. Aravindan · P. Vickraman · A. Sivashanmugam · R. Thirunakaran · S. Gopukumar

Received: 2 December 2008 / Accepted: 18 June 2009

Abstract Polyvinylidenefluoride–hexafluoropropylene-based (PVdF–HFP-based) gel and composite microporous membranes (GPMs and CPMs) were prepared by phase-inversion technique in the presence 10 wt% of $AlO(OH)_n$ nanoparticles. The prepared membranes were gelled with 0.5-M $LiPF_3(CF_2CF_3)_3$ (lithium fluoroalkylphosphate, LiFAP) in EC:DEC (1 : 1 v/v) and subjected to various characterizations; the AC impedance study shows that CPMs exhibit higher conductivity than GPMs. Mechanical stability measurements on these systems reveal that CPMs exhibit Young's modulus higher than that of bare and GPMs and addition of nanoparticles drastically improves the elongation break was also noted. Transition of the host from α to β phase after the loading of nanosized filler was confirmed by XRD and Raman studies. Physico-chemical properties, like liquid uptake, porosity, surface area, and activation energy, of the membranes were calculated and results are summarized. Cycling performance of Li/CPM/$LiFePO_4$ coin cell was fabricated and evaluated at $C/10$ rate and delivered a discharge capacity of 157 and 148 mAh g^{-1} respectively for first and tenth cycles.

PACS 82.47.Aa · 82.45.Mp · 82.45.Gj · 72.80.Le · 84.37.+q

1 Introduction

The plastic lithium ion (PLiON) batteries offer the shape versatility, flexibility, and lightness which can be commercialized since it accommodates the miniature and electronic industries, like computers, camcorders, mobile societies, etc. [1]. These could be possible with an evident use of polymer electrolyte as separators. So, the search for finding suitable polymer electrolytes satisfying high ionic conductivity, good mechanical, thermal, interfacial, and electrochemical stabilities is evinced. Generally, two methods of preparation have been adopted to prepare the polymer electrolytes:

– First and most common approach is by dissolving the salts into polymer host (called solid polymer electrolytes [SPEs]) and the incorporation of low molecular weight liquids, like ethylene carbonate, diethyl carbonate, dimethyl carbonate, etc., into said host (called gel polymer electrolytes [GPEs]), both were prepared by solution casting technique in a single-step process. This method has certain drawbacks including simultaneous loss of mechanical stability; gas evolution during cycling, etc. which hinders the possibility of using in practical batteries. In order to overcome such drawbacks that occurred in the above electrolytes without affecting the conductivity, the nanosized inorganic filler has been incorporated. The addition of such nanoparticles not only improves the conductivity which also enhances aforesaid requisites [2, 3].

V. Aravindan · P. Vickraman (✉)
Department of Physics, Gandhigram Rural University, Gandhigram 624 302, India
e-mail: vrsvickraman@yahoo.com
Fax: +91-451-2454466

V. Aravindan
e-mail: aravind_van@yahoo.com

Present address:
V. Aravindan
The Research Institute for Catalysis, Chonnam National University, Gwang-ju 500-757, Republic of Korea

A. Sivashanmugam · R. Thirunakaran · S. Gopukumar
Electrochemical Energy Systems Division, Central Electrochemical Research Institute, Karaikudi 630 006, India

Published online: 04 July 2009

However, the possibilities of using these electrolytes are limited due to the poor ionic conductivity and leakage problems of SPEs and GPEs, respectively.

– In the second method, Tarascon et al. [4] explored the preparation of porous electrolyte membranes by two step processes. In the first step process, a film was formed by evaporating the casting polymer solution and in the second step (activation process) the soaking of the film into electrolyte solutions [4]. This two step process, the extraction of dibutylpthalate was found to be very difficult, which increase the cost of the membranes and safety issues while handling large amounts of volatile solvents [5]. Later, to overcome these difficulties Tarascon et al. [5], Saito et al. [6], and Wang et al. [7] independently attempted to prepare the microporous membranes by phase inversion using solvents and nonsolvents. Very recently, Kim et al. [8–11] also prepared porous membranes by the same technique, but with various kinds of nanoparticles, such as TiO_2 (rutile and anatase), SiO_2, and Al_2O_3.

The commercially usable $LiPF_6$-based electrolyte containing lithium ion batteries encountered certain drawbacks [12–16]. To overcome these shortcomings, the salt is modified in such a way that the replacement of PF_6^- in $LiPF_6$ by $-CF_2CF_3$ groups stabilizes the anion [12, 13] and $PF_3(CF_2CF_3)_3^-$ is more stable than PF_6^-; the modified one does not undergo hydrolysis readily as PF_6^- or its decomposition product, PF_5. Consequently lithium fluoroalkylphosphate ($LiPF_3[CF_3CF_2]_3$) (LiFAP) electrolytes contains much less HF contamination than $LiPF_6$ [12]. Gnanaraj et al. [14–16] reported the possibility of using LiFAP based electrolytes in $LiMn_2O_4$. The main advantage of using LiFAP is the surface of the electrodes is dominated by the solvent reduction products whereas $LiPF_6$-based electrolytes dominate by salt reduction products leads to the different surface chemistry [14]. In this present study, we report preparation of the composite polymer membranes by phase-inversion technique (CPMs). The polyvinylidenefluoride–hexafluoropropylene (PVdF–HFP) is a very promising host for phase-inversion technique due to its appealing properties is selected [4–11, 13]. For the first time, LiFAP has been used to gellify the polymer skeleton in the presence of 10 wt% $AlO(OH)_n$ nanoparticles with $Li/LiFePO_4$ configuration.

2 Materials and methods

2.1 Materials

PVdF–HFP with 12 mol% of HFP (Solvay Solexis, Italy); $AlO(OH)_n$ (Candia, Taiwan); $LiFePO_4$ (Hydro Quebec, Canada); $LiPF_3(CF_3CF_2)_3$ (Merck KGaA, Germany); ethylene carbonate, diethyl carbonate, acetone, ethanol, and *n*-butanol (E. Merck, India) were used as received. Acetone to ethanol ratio was fixed at 5 : 1 for the preparation of bare PVdF–HFP polymer membranes. Composite polymer membranes (CPM) were cast with $AlO(OH)_n$ nanoparticle in an optimized concentration of 10 wt%. PVdF–HFP was dissolved in a mixture of solvent (acetone, E. Merck India) and nonsolvent (ethanol, E. Merck India) such that amount of the nonsolvent was low enough to allow solubilization and high enough to allow phase separation upon evaporation (solvent and nonsolvent ration was fixed 5 : 1 ratio). The resulting suspension was spread on a glass substrate and allowed to evaporate the solvent and nonsolvent in turn in the air atmosphere with 60–100 μm thickness. Then the membrane was dried and transferred into Ar-filled glove box for gellification of 0.5-M LiFAP in EC:DEC (1 : 1 v/v) solution. Further, the electrolytic uptake and porosity measurements were performed by using 0.5-M LiFAP in EC:DEC (1 : 1 v/v) and *n*-butanol with high purity which were purchased from E. Merck, India. and used as without further purification.

2.2 Instrumentation

Morphological features of the polymer membranes were examined using a Hitachi Model S-3000H scanning electron microscope (SEM). Ionic conductivities of the membranes were observed by AC impedance spectroscopy in the frequency range 1 Hz to 5 MHz in a Solartron 1260 Impedance/Gain Phase Analyzer coupled with a Solartron Electrochemical Interface using a stainless steel blocking electrode impedance cell of 1 cm^2 area. Differential scanning calorimetric studies of the polymer membranes were recorded using a Perkin Elmer Pyris 6 instrument under nitrogen atmosphere between 50 and 250°C at a heating rate of 10°C/min. Instron Corporation series IX automated mate were used to measure the mechanical strength of the polymer membranes. The surface area and pore size of the membranes were determined by a continuous flow nitrogen gas adsorption/desorption BET apparatus (Gemini, Micromeritics, USA).

2.3 Coin cell assembly

Coin cells of 2016 configuration were assembled using lithium metal as an anode, $LiFePO_4$ as a cathode, and composite polymer membranes as separator–cum–electrolyte soaked in 0.5-M LiFAP in EC: DEC (1 : 1 v/v) for 1 h. The cathodes comprising $LiFePO_4$ (60%), carbon black (30%), and PVdF binder (10%) were prepared by a slurry coating process over the aluminum foil using doctor blade. The *N*-methyl pyrrolidone (NMP) was used as slurrying agent during the preparation. The coated aluminum foil was dried in an oven at 110°C for 2 h and pressed under a pressure of 12 t $kg\,cm^{-2}$ for 3 min. 18-mm diameter blanks were punched out from the coated area and used as cathode. Coin

cells were assembled inside an argon-filled glove box (M Braun, Germany) and subjected to electrochemical cycling studies.

2.4 Cycling studies

Cycling behavior of Li/LiFePO$_4$ cells with polymer electrolyte membranes as a separator was performed galvanostatically in a computerized battery cycling unit at C/10 rate between the potential windows 2.5–4.5 V.

3 Results and discussion

3.1 Thermal studies

High ionic conductivity, high lithium transport number, wider electrochemical stability, and mechanical stability are envisaged as desirable properties, are not sufficient for its end use of polymer electrolyte as separator as well as electrolyte for practical applications because thermal stability is also one of the important factors to guarantee acceptable performance of it, while it is operated at elevated temperatures. In this connection, differential scanning calorimetry (DSC) study has been carried out to analyze the thermal stability of the polymeric membranes.

Figure 1 shows the DSC thermograms of pure PVdF–HFP, gelled (GPMs), and CPMs. The melting endotherm (T_m) of pure membrane is observed at 137.03°C is due to the melting of dominant α VdF crystalline phase and shift in T_m towards lower temperature at 109.70°C of the host after the gellation (GPM) is noted. As far as CPM concerned T_m shifts towards the higher temperature (119.19°C) due to the addition of AlO(OH)$_n$ nanoparticles which is found to be having better stability than GPMs. Percentage of crystallinity of the membranes are calculated from thermal traces using $\chi_c = \frac{\Delta H_m}{\Delta H_m^o}$, where, ΔH_m^o is the reference heat of fusion (104.7 J/g) for pure α phase crystals of PVdF and ΔH_m is heat of fusion of such membranes [17]. The crystalline strands 28, 19, and 16% are calculated respectively for pure, GPMs, and CPMs. This shows that addition of nanoparticles prevents the reorganization of polymer chains leads to decrease in crystallinity [17].

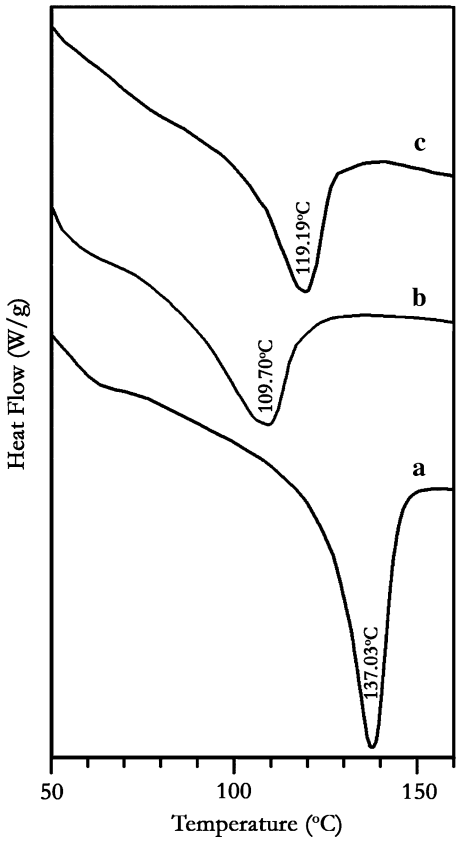

Fig. 1 Differential scanning calorimetric traces of **a** bare, **b** gel, and **c** composite PVdF–HFP membranes

3.2 Mechanical stability

The addition of inorganic filler particles in polymeric materials is to enhance the toughness is well known. Practically, the focus is to maximize interaction between the polymer matrix and ceramic particles [18], which called for the use of small particles that provide high surface area for interaction with the polymer host [19, 20]. Thus, the incorporation of nanoparticles in polymeric materials induces structural and morphological changes and facilitates the improved mobility for ions. Figure 2 depicts the stress-strain behavior of polymer membranes for pure PVdF–HFP, GPMs, and that of with AlO(OH)$_n$ nanoparticles. It could be observed that the Young's modulus decreases for GPMS from 4.3 to 4.1 MPa after gellation and for CPM it is found to be around 5.87 MPa, while the elongation breaks 71.5, 122.43, and 319%, respectively for GPM, pure PVdF–HFP, and CPM are noted. Thus, incorporation of 10% AlO(OH)$_n$ in the electrolyte shows an improvement in their mechanical stability. Hitherto, the improved mechanical stability may be ascribed to the high mobility of AlO(OH)$_n$ nanoparticles under the applied stress, which helps in dissipation of energy to the host. Gersappe [21] showed by molecular simulations of polymers reinforced with nanosized fillers that it is not only the surface area, but also the mobility of the nanofillers which controls the ability to dissipate energy, providing improved toughness to the composite membrane. A similar improvement in toughness has been observed by Shah et al. [22, 23], who investigated the effect of layered SiO$_2$ nanoparticles on PVdF and polystyrene polymer hosts.

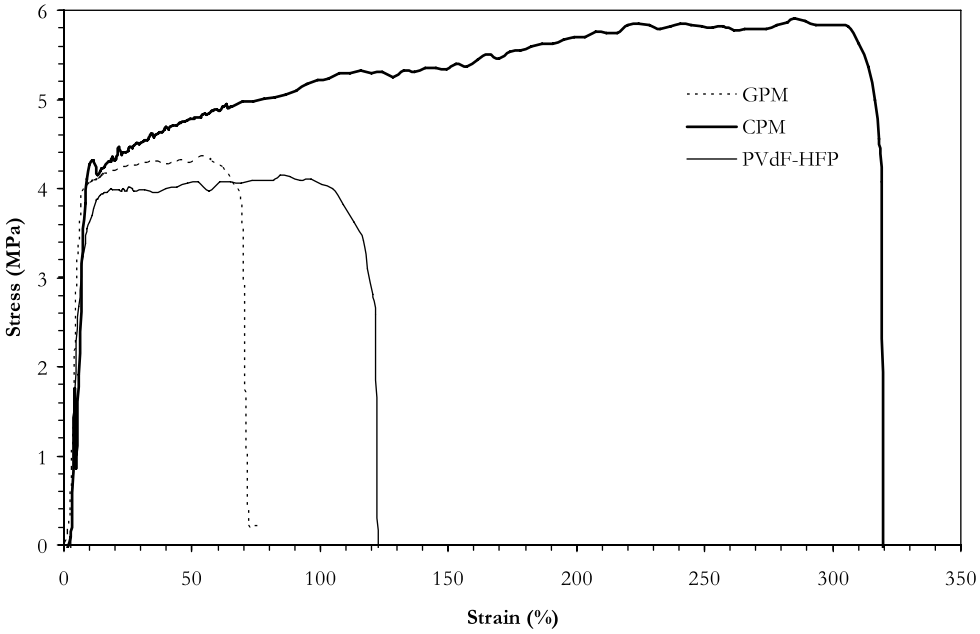

Fig. 2 Stress-strain curves of **a** bare, **b** gel, and **c** composite PVdF–HFP polymeric membranes

3.3 Raman studies

Raman analysis was carried out to confirm the formation of the β phase after the addition of the ceramic filler. The Raman spectrum was recorded with pure PVdF–HFP, GPMs, and CPMs having 10 wt% of $AlO(OH)_n$ (Fig. 3). The bands at 795 and 950 cm^{-1} are corresponding to the CH_2 rocking and twisting vibrations, respectively, of the α phase is clear. The shifting of band at 873 cm^{-1} for the combination of symmetric C–C band and CCCδ skeletal bending of C(F)–C(H)–C(F) [24] are also be observed. The appearance of very strong band for the CPM at 898 cm^{-1} is due to the –OCOO– out of plane deformation of DEC [25]. The appearance of a peak at 838 cm^{-1} in CPMs confirms the formation of the polar β phase [24]. In the β conformation, the fluorine and the hydrogen atoms are so arranged that the dipole moment per unit cell is maximized. The change into the polar β conformation suggests some kind of separation of hydrophilic and hydrophobic sites, which can affect the morphology and functionality of the membrane.

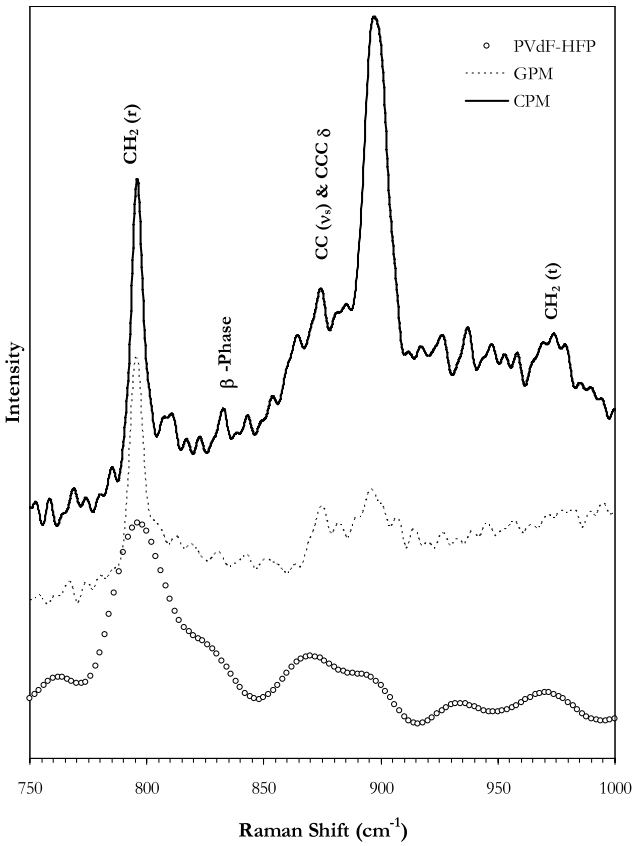

Fig. 3 Raman spectrums of **a** bare, **b** gel, and **c** composite PVdF–HFP polymeric membranes

3.4 Ionic conductivity

The temperature dependence of the ionic conductivity is presented in Fig. 4. Ionic conductivity of membrane is calculated from the following equation

$$\sigma = \frac{l}{R_b r^2 \pi} \tag{1}$$

where l and r represent the thickness and the radius of the sample membrane disk, respectively. R_b is the bulk resistance obtained from AC impedance measurements. It is obviously observed that addition of nanoparticulate $AlO(OH)_n$ substantially enhances the conductivity. The conductivities of 1.57 and 3.57 mS cm^{-1} are observed for gel and composite membranes, respectively.

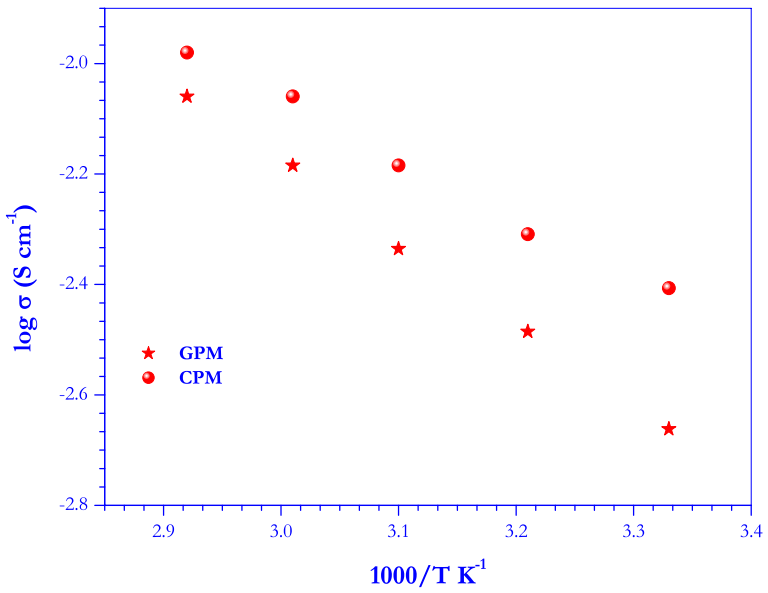

Fig. 4 Temperature dependence of ionic conductivity of the polymeric membranes

The enhancement of conductivity may be attributed to the Lewis acid–base interaction between the OH^- groups of the nanoparticulate $AlO(OH)_n$ and F atoms of the polymer molecules, which prevents the reorganization of polymer chains making vast amorphous domain resulted in higher electrolyte uptake than GPM at ambient temperature conditions [17]. The aforementioned interaction promotes the dissociation of salts via the sort of "ion-filler" complex formation [26]. As the temperature increases, the increasing trend of conductivity is also noted.

3.5 XRD studies

X-ray diffraction measurements were made to examine the crystallinity and complexation relative to the host polymer. X-ray diffraction patterns of the composite polymer electrolytes (Fig. 5) reveal the dominant crystal phases of PVdF–HFP. The appearance of characteristic peak at ∼26° attributed to the crystalline phase of VdF crystals. After the gellation of the membranes (GPMs), the crystalline nature of the membranes is tend to decrease whereas in the case of CPMs, the band is shifted and splitted, this favors the formation of fibrous β phase. This infers that addition of $AlO(OH)_n$ nanoparticles leads to prevent the reorganization of the polymer chains resulted in improved amorphousity [17]. This kind of reorganization is not observed in the case of GPMs.

3.6 Physico-chemical properties

The various physico-chemical properties of the gelled and composite PVdF–HFP membranes are summarized in Table 1 and the calculations are made according to

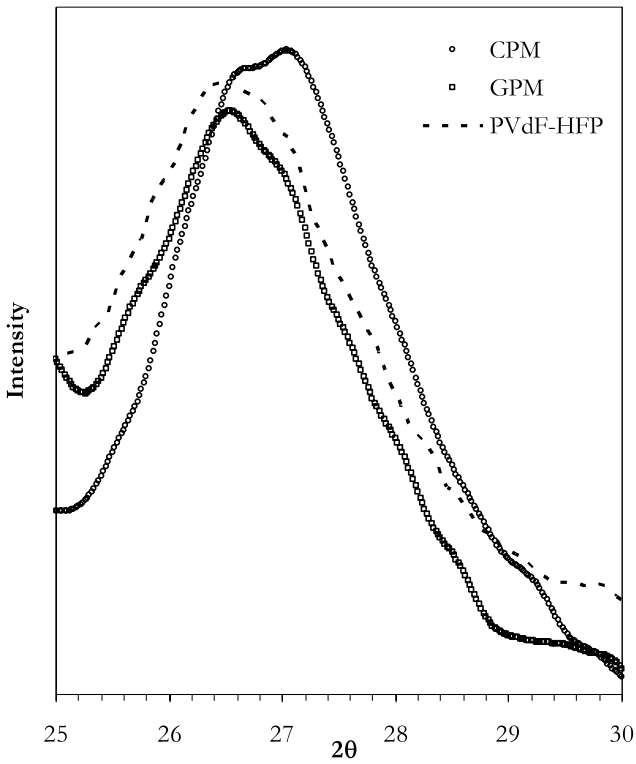

Fig. 5 X-ray diffraction patterns of **a** bare, **b** gel, and **c** composite PVdF–HFP polymeric membranes

Li et al. [17]. It is evident from the table that composite PVdF–HFP membranes possess superior physico-chemical characteristics, like higher liquid uptake, porosity, and surface area. It is found that the pore formation of CPMs showed more pore formation and higher electrolyte uptake than the GPEs which may be due to the interfacial layers between nanoparticulate $AlO(OH)_n$ and Polymer matrix . The

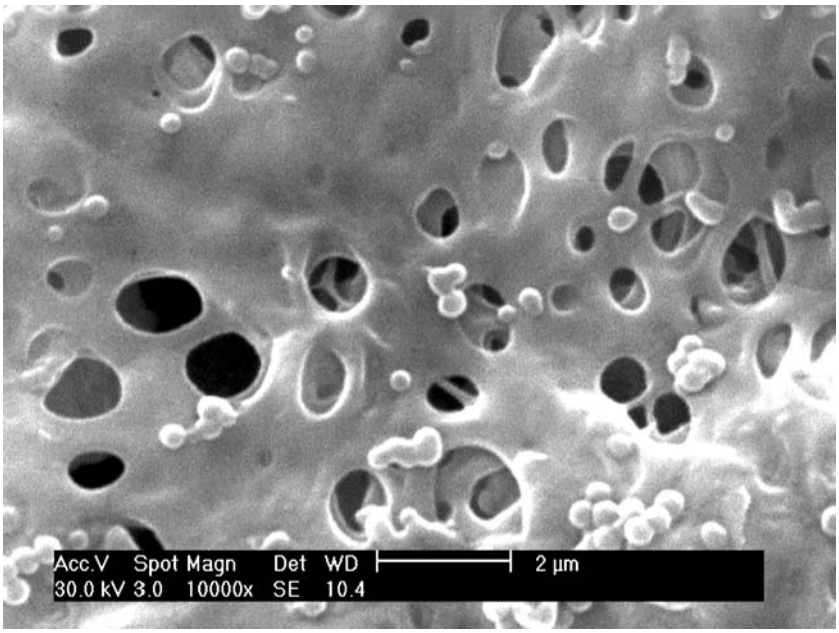

Fig. 6 Scanning electron microscopic images of composite PVdF–HFP membranes

Table 1 Physico-chemical properties of gel (GPMs) and composite (CPMs) PVdF–HFP membranes

Physico-chemical properties	GPM	CPM
Liquid uptake (%)	164	194
Porosity (%)	60	65
Crystallinity (%)	19	16
Activation energy (kJ mol^{-1})	7.47	7.38
Surface area (m^2 g^{-1})	19.4	27.7

calculated porosities are 65 and 60%, respectively for CPM and GPM membranes (Table 1). In addition, these membranes exhibit relatively low crystallinity and lower activation energy which are essential for better ionic conductivity so as to enable to use it as a prospective polymer film in energy storage device applications.

3.7 Morphological studies

A morphological feature of the membrane was analyzed by scanning electron microscope (SEM) (Fig. 6). It can be seen that the membranes exhibited highly porous in nature with embedded nanoparticulate $AlO(OH)_n$ (possible swelling mechanisms are given in Scheme 1). After the activation of CPM with electrolyte solution, i.e., 0.5-M LiFAP in EC:DEC (1 : 1 v/v) gives rise to multiphase systems that result in amorphous swollen gel, crystalline strands and the cavities filled with solutions (liquid phase). The membrane's porosity, amount of solution uptake, pore size, interconnectivity, the conductivity of the electrolyte (i.e., solution and the extent to which the electrolyte wets the pore walls of the membrane) clearly seen which are important factors in determining the ionic conductivity of the membrane [27–29]. These properties are promising one as the basic pore size requisite for the separator in lithium batteries is <1 µm and porosity is ~40% (Celgard) [30]. In the morphological studies, the CPMs show good wetability for liquid uptake. As a result CPMs are generally expected to facilitate faster ionic transport, high ionic conductivity, low bulk impedance, and high rate capability, which render them as suitable candidate for lithium ion cells of high power density.

3.8 Charge–discharge studies

Gnanaraj et al. [14–16, 31, 32] extensively studied LiFAP-based electrolyte solutions in graphite and $LiMn_2O_4$ electrodes. The results showed that the partial replacement of fluorine atoms by fluoroalkyl groups substantially enhanced the cycling performance of the cell than $LiPF_6$ and $LiN(CF_2CF_3SO_2)_2$ in EC:DEC:DMC (2 : 1 : 2) solution at ambient temperature. The irreversible capacity of the LiFAP-based electrolyte was found less than $LiPF_6$ than other electrolytes. Furthermore, surface of the electrodes were dominated by the solvent reduction species, i.e., polymerization of the solvent molecule to derivatives of polyethyleneoxide, polycarbonates occur in LiFAP-based solutions results higher capacity and stability (upon cycling) of the electrodes [14].

The cycling performances of Li/CPM/$LiFePO_4$ cells were studied glavanostatically and the typical charge–discharge curves are presented in the Fig. 7. It is clear that these cells exhibit flat charge–discharge characteristics showing plateau regions around 3.6 and 3.2 V during the cycling. The observed profiles are very similar to that of

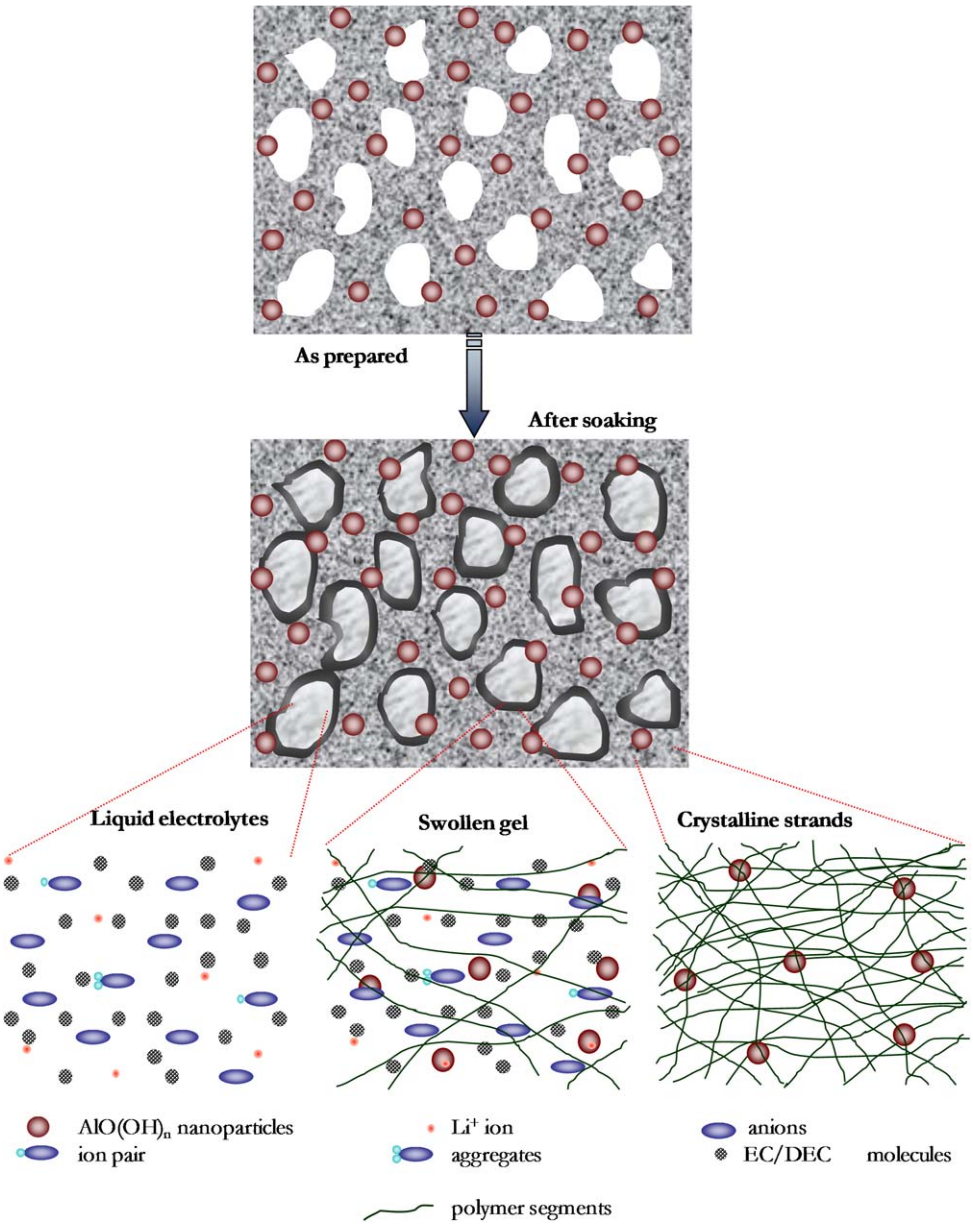

Scheme 1 Schematic representation of multiphase system

Li/LiFePO$_4$ cells employing Celgard separator. This shows that the polymer membrane holds good stability to act as a separator as well as a potential electrolyte. Figure 8 shows the discharge capacity obtained from Li/CPM/LiFePO$_4$ cells with number of cycles. It is obvious that over the investigated ten cycles, these cells exhibit stable discharge behavior. These cells delivered a specific discharge capacity of 157 and 148 mAh g^{-1} at the first and tenth cycle discharged at $C/10$ rate. The cells experience a capacity fade of 0.9 mAh g^{-1} cycle^{-1} over the investigated ten cycles. The fade in capacity may be ascribed to the formation of the surface films as in the case of $LiMn_2O_4$ electrodes. The formation of such films is beneficial for the electrodes in the sense that it offsets the further unwanted reaction with the electrolyte and prevents self-discharge [1].

The studies revealed that AlO(OH)$_n$ filled PVdF–HFP polymer membranes could be potentially exploited as an efficient separator-cum-electrolyte component in lithium batteries in conjunction with LiFePO$_4$ counterpart.

4 Conclusions

Lithium-fluoroalkylphosphate-based composite polymer membranes were prepared by phase-inversion technique with AlO(OH)$_n$ nanoparticles as filler. The membranes were characterized through different techniques to find out their thermal stability, mechanical strength, surface morphology, porosity, ionic conductivity, etc. Addition of AlO(OH)$_n$ nanoparticles into the PVdF–HFP network improves the

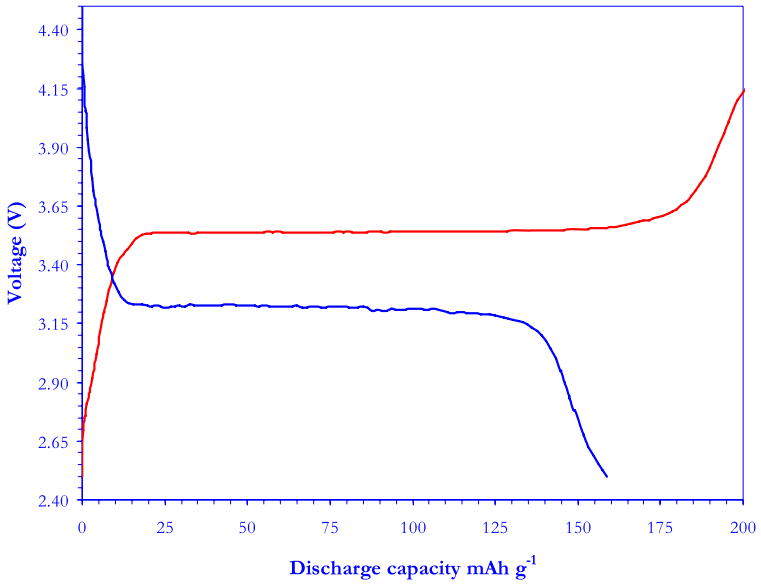

Fig. 7 Charge–discharge profile of Li/CPM/$LiFePO_4$ cell at $C/10$ rate

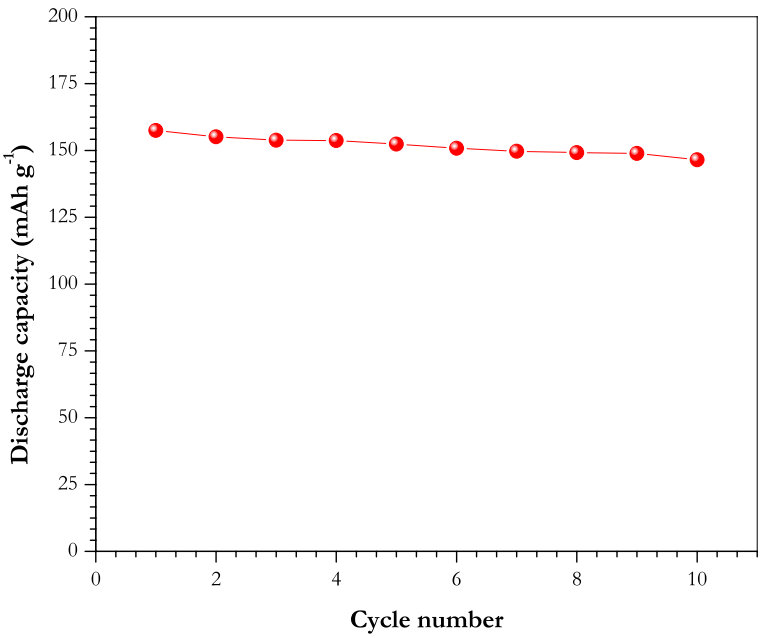

Fig. 8 Plot for discharge capacity with cycle number of Li/CPM/$LiFePO_4$ cell

physical properties of the membranes. An attempt has been made to use these membranes as a separator-cum-electrolyte in a Li/$LiFePO_4$ cells [33]. The 2016 configuration coin cells were assembled and their cycling performances have been evaluated. It is evident that over the investigated ten cycles, these cells exhibit stable discharge behavior. The cells delivered a specific discharge capacity of 157 and 148 mAh g^{-1} at first and tenth cycle discharged at $C/10$ rate. The cells experience a capacity fade of 0.9 mAh g^{-1} $cycle^{-1}$ over the investigated ten cycles. The studies suggested that $AlO(OH)_n$ filled PVdF–HFP polymer membranes could be promising candidate to be used as separator–cum–electrolyte component in lithium batteries.

Acknowledgements One of the authors (V.A.) wishes to thank Dr. Karim Zaghib, Hydro Quebec, Canada, and Mrs. Anna Maria Bertasa, Solvay Solexis, Italy, for kindly providing chemicals. The author is also grateful to the Council of Scientific and Industrial Research (CSIR), New Delhi, India, for the award of Senior Research Fellowship.

References

1. J.M. Tarascon, M. Armand, Nature **414**, 359 (2001)
2. F. Croce, G.B. Appetecchi, L. Persi, B. Scrosati, Nature **394**, 456 (1998)
3. M.M.E. Jacob, E. Hackett, E.P. Giannelis, J. Mater. Chem. **13**, 1 (2003)
4. J.M. Tarascon, A.S. Gozdz, C. Schmutz, F. Chmutz, F. Shokoohi, P.C. Warren, Solid State Ion. **86–88**, 49 (1996)

5. A. Du Pasquier, P.C. Warren, D. Culver, A.S. Gozdz, G.G. Amatucci, J.M. Tarascon, Solid State Ion. **135**, 249 (2000)
6. Y. Saito, H. Kataoka, A.M. Stephan, Macromolecules **34**, 6955 (2001)
7. C.C. Wang, C.C. Wan, Y.Y. Wang, Electrochem. Commun. **6**, 531 (2004)
8. K.M. Kim, N.G. Park, K.S. Ryu, S.H. Chang, Electrochim. Acta **51**, 5636 (2006)
9. K.M. Kim, N.G. Park, K.S. Ryu, S.H. Chang, J. Appl. Polym. Sci. **102**, 140 (2006)
10. K.M. Kim, J.C. Kim, K.S. Ryu, Macromol. Mater. Eng. **291**, 1495 (2006)
11. K.M. Kim, J.C. Kim, K.S. Ryu, Macromol. Chem. Phys. **208**, 887 (2007)
12. M. Schmidt, U. Heider, A. Kuehner, R. Oesten, M. Jungnitz, N. Ignat'ev, P. Sartori, J. Power Sources **97–98**, 557 (2001)
13. V. Aravindan, P. Vickraman, Eur. Polym. J. **43**, 5121 (2007)
14. J.S. Gnanaraj, E. Zinigrad, L. Asraf, M. Sprecher, H.E. Gottlieb, W. Geissler, M. Schmidt, D. Aurbach, Electrochem. Commun. **5**, 946 (2003)
15. J.S. Gnanaraj, M.D. Levi, Y. Gofer, D. Aurbach, M. Schmidt, J. Electrochem. Soc. **150**, A445 (2003)
16. D. Aurbach, J.S. Gnanaraj, W. Geissler, M. Schmidt, J. Electrochem. Soc. **151**, A23 (2004)
17. Z. Li, G. Su, D. Gao, X. Wang, X. Li, Electrochim. Acta **49**, 4633 (2004)
18. G. Kraus, *Reinforcement of Elastomers*. Interscience, New York (1965)
19. V. Aravindan, P. Vickraman, Solid State Sci. **9**, 1069 (2007)
20. Z.S. Petrovic, W. Zhang, Mater. Sci. Forum **352**, 171 (2000)
21. D. Gersappe, Phys. Rev. Lett. **89**, 058301 (2002)
22. D. Shah, P. Maiti, E. Gunn, D.F. Schmidt, D.D. Jiang, C.A. Batt, E.P. Giannelis, Adv. Mater. **16**, 1173 (2004)
23. D. Shah, P. Maiti, D.D. Jiang, C.A. Batt, E.P. Giannelis, Adv. Mater. **17**, 525 (2005)
24. R.D. Simoes, A.E. Job, D.L. Chinaglia, V. Zucolotto, J.C.C. Filho, N. Alves, J.A. Giacometti, O.N. Oliveira, Jr., C.J.L. Constantino, J. Raman Spectrosc. **36**, 1118 (2005)
25. J. Wang, Y. Wu, X. Xuan, H. Wang, Spectrochim. Acta A **58**, 2097 (2002)
26. A.M. Stephan, K.S. Nahm, M.A. Kulandainathan, G. Ravi, J. Wilson, J. Appl. Electrochem. **36**, 1091 (2006)
27. S.W. Choi, S.M. Jo, W.S. Lee, Y.R. Kim, Adv. Mater. **15**, 2027 (2003)
28. C. Capiglia, Y. Saito, H. Kataoka, T. Kodama, E. Quartarone, P. Mustarelli, Solid State Ion. **131**, 291 (2000)
29. J. Xi, X. Qiu, L. Chen, Solid State Ion. **177**, 709 (2005)
30. P. Arora, Z. Zhang, Chem. Rev. **104**, 4419 (2004)
31. J.S. Gnanaraj, E. Zinigrad, E. Levi, D. Aurbach, M. Schmidt, J. Power Sources **119–121**, 799 (2003)
32. E. Zinigrad, L. Asraf, J.S. Gnanaraj, H.E. Gottlieb, M. Sprecher, D. Aurbach, J. Power Sources **146**, 176 (2005)
33. V. Aravindan, Ph.D. thesis, Gandhigram Rural University, Gandhigram 624302, India, 2008